VA-491-050-TR

NOVEL ACOUSTIC TECHNIQUE FOR UXO DISCRIMINATION

FINAL REPORT
SERDP EXPLORATORY DEVELOPMENT (SEED) PROJECT CU-1172

Dr. Thomas Bell
AETC Incorporated

Prof. Nenad Gucunski
Rutgers University

June 30, 2001

This material is based upon work supported by the U. S. Army Corps of Engineers under contract number DACA72-00-P-0059. Any opinions, findings and conclusions or recommendations expressed in this material are those of the authors and do not necessarily reflect the views of the U. S. Army Corps of Engineers.

Report Documentation Page

Form Approved
OMB No. 0704-0188

1. REPORT DATE	2. REPORT TYPE	3. DATES COVERED
30 JUN 2001		**00-00-2001 to 00-00-2001**

4. TITLE AND SUBTITLE	5a. CONTRACT NUMBER
Novel Acoustic Technique for UXO Discrimination	5b. GRANT NUMBER
	5c. PROGRAM ELEMENT NUMBER
6. AUTHOR(S)	5d. PROJECT NUMBER
	5e. TASK NUMBER
	5f. WORK UNIT NUMBER
7. PERFORMING ORGANIZATION NAME(S) AND ADDRESS(ES) **AETC Incorporated,8910 University Center Ln., Ste. 900,San Diego,CA,92122**	8. PERFORMING ORGANIZATION REPORT NUMBER
9. SPONSORING/MONITORING AGENCY NAME(S) AND ADDRESS(ES)	10. SPONSOR/MONITOR'S ACRONYM(S)
	11. SPONSOR/MONITOR'S REPORT NUMBER(S)

12. DISTRIBUTION/AVAILABILITY STATEMENT
Approved for public release; distribution unlimited

13. SUPPLEMENTARY NOTES

14. ABSTRACT

15. SUBJECT TERMS

16. SECURITY CLASSIFICATION OF:			17. LIMITATION OF ABSTRACT	18. NUMBER OF PAGES	19a. NAME OF RESPONSIBLE PERSON
a. REPORT	b. ABSTRACT	c. THIS PAGE			
unclassified	**unclassified**	**unclassified**	**Same as Report (SAR)**	**18**	

Contents

1. Introduction

Recent demonstrations have shown that magnetic and electromagnetic induction technology can reliably detect most buried unexploded ordnance (UXO). Unfortunately, current technology is unable to reliably discriminate between UXO and other items that pose no risk, and typical survey methods currently deployed have an excessive level of false alarms (i.e. marking of sub-surface anomalies that do not correspond to UXO). There is a need for systems that, when cued by standard survey technologies, can cost effectively, non-invasively interrogate the suspected item and discriminate.

One distinguishing characteristic of UXO is its shape: projectiles, mortars, bombs and rockets are characteristically long and slender. Over the past few years, several Strategic Environmental Research and Development Program (SERDP) and Environmental Security Technology Certification Program (ESTCP) sponsored projects have shown varying degrees of success in developing techniques for using magnetics and electromagnetic induction to discriminate between different target shapes [1]. This report documents the results of a SERDP Exploratory Development (SEED) project that applies a complementary sensor technology to the problem. The objective of the project was to demonstrate that relatively simple seismic technology routinely used for pavement and soil mechanical analysis can be used for classification and discrimination of buried objects.

This report has six sections. Following this introduction, section 2 gives the background for the project, and the basic concept is described in section 3. Details of the experimental work done for this project are documented in section 4, and our conclusions are presented in section 5. Section 6 lists references cited in the report. Because of shortcomings of the instrumentation used in this project, the results are not conclusive. We measured signals that are qualitatively similar to those expected on the basis of numerical studies, but the spatial and frequency resolution was not good enough to support quantitative evaluation of the effects.

2. Background

SERDP has funded some research on seismic techniques for buried UXO detection and classification at BBN Technologies. The emphasis of that research was on acoustic imaging and exploiting spectral characteristics of the acoustic response for target classification. The basic idea is that a sufficiently detailed acoustic image should reveal the location and shape of the target, while the spectral response should reveal patterns of structural resonances that are uniquely related to the shape and composition of the target. Their results to date were reported recently at the 1998 and 1999 SERDP Symposia and the UXO/Countermine Forum [2]. System simulations indicate that a roughly 3 m by 3 m array with about 100 geophones, ringed by 9 seismic sources (bandwidth 5-800 Hz) can provide useful target location and shape information for targets of size on the order of 20 cm. Finite element modeling of the elastic response of ordnance items has identified modal lines or resonances at 1.57 kHz and higher for 155 mm projectiles. Measurements of the acoustic response of a buried 155 mm projectile shows modal lines similar to model results.

Here, we focus on an approach to seismic classification and discrimination that does not rely on detailed imaging or structural resonances. Our interest in this approach derives primarily from experience in the detection and location of underground obstacles by the SASW (Spectral Analysis of Surface Waves) method [3]. The SASW procedure is routinely used for non-invasive evaluation of elastic moduli and layer thicknesses in layered media such as soils and pavements. SASW testing uses a simple configuration consisting of an impact source and a pair of geophones to measure the dispersion of seismic surface (Rayleigh) waves. The shear wave velocity profile is estimated by inverting the measured Rayleigh wave dispersion curve.

The application of SASW techniques to detection and classification of buried objects has evolved from the results of numerical simulations of the SASW method [4]. The numerical studies were conducted on finite element models of a soil stratum with obstacles of various sizes, shapes and densities (buried objects and cavities). Several important observations were made from results simulating a movement of a pair of receivers (similar to the SASW testing) in the direction of the buried object. The most important observation was that an object or a cavity causes fluctuations in the dispersion curve. The fluctuations are caused by reflections of both surface and body waves from the obstacle. The intensity of fluctuations increases as the receiver spacing decreases and as the receiver pair approaches the obstacle. The fluctuations vanish as the receiver pair passes the obstacle. The second important observation was that, if the receiver pair is placed so that it straddles the buried object, there is a general increase in the phase velocity of the dispersion curve for rigid obstacles, and a decrease for soft obstacles or cavities.

3. The SASW Technique

The standard SASW test setup is illustrated schematically in figure 1. An impact source S generates a spectrum of elastic waves that are measured by a pair of receivers R_1 and R_2. We are interested in interference effects, due to waves scattered by the target T, in the frequency-dependent phase shift between the signals at the two receivers. The phase shift is calculated directly from the cross-spectrum of the signals at the two receivers. Normally (i.e., when there is nothing buried in the ground) this phase shift is used to calculate the Rayleigh wave phase speed as a function of frequency. Our work is based on the premise that, when viewed over a range of target aspect angles, the frequency dependent phase shifts among the signals measured at several receivers contain a unique "signature" of the target that can be exploited to discriminate between buried UXO and clutter. This target signature will also depend on target size and depth and on the source-receiver geometry in relationship to the target (x, y) location. However, these are known and/or controlled variables. Target location, size and depth can usually be accurately estimated from the cueing sensor data [a], and the sensor geometry can be adjusted as appropriate.

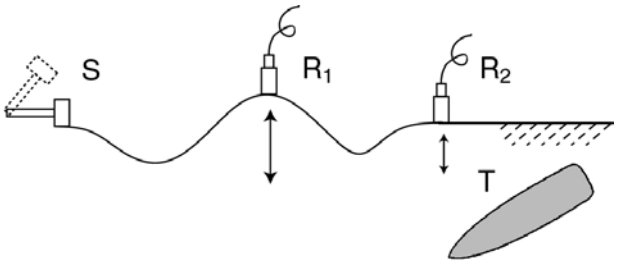

Figure 1. Schematic of SASW seismic test with impact source (S) and two accelerometers (R_1 and R_2) and a buried target (T).

In the simple two-dimensional case, ignoring mode conversion and attenuation, the vertical velocity at the surface can be expressed as

$$v(x,t) = \frac{1}{2\pi}\int \{v_0(\omega)e^{-i[k(\omega)x-\omega t]} + v_1(\omega)e^{i[k(\omega)x+\omega t]}\}d\omega \qquad (1)$$

where v_0 corresponds to the wave generated by the source and v_1 corresponds to the wave scattered by the target. In this expression, $k = 2\pi/\lambda$ is the wavenumber. Although this is a simplified representation, it suffices to illustrate how we will approach the problem. The model can easily accommodate attenuation and spreading in the full three-dimensional case.

To first order in the scattered amplitude, the cross spectrum of the signals at two measurement points is

$$\hat{V}(x_1,\omega)\hat{V}^*(x_2,\omega) = v_0 v_0^* e^{-ik(x_1-x_2)} + v_0 v_1^* e^{-ik(x_1+x_2)} + v_0^* v_1 e^{ik(x_1+x_2)} \qquad (2)$$

where * indicates the complex conjugate and ^ indicates the Fourier Transform. If we express the scattered wave amplitude in terms of a complex-valued reflection coefficient β, then equation (2) becomes

$$\hat{V}(x_1,\omega)\hat{V}^*(x_2,\omega) = v_0 v_0^* \{e^{-ik(x_1-x_2)} + \beta e^{ik(x_1+x_2+2x_T)} + \beta^* e^{-ik(x_1+x_2+2x_T)}\}. \qquad (3)$$

In equation (3), x_T is the distance from the far receiver (R_2 in figure 1) to the target. The phase γ of the cross spectrum is given by

$$\gamma = \mathrm{Ph}\left(\hat{V}(x_1,\omega)\hat{V}^*(x_2,\omega)\right)$$
$$= \tan^{-1}\left(\frac{\sin[k(x_2 - x_1)]}{\cos[k(x_2 - x_1)] + 2\,\mathrm{Re}\{\beta \exp[ik(x_1 + x_2 + 2x_T)]\}}\right). \quad (4)$$

With no obstacle, $\gamma(\omega) = k(\omega)\Delta x$, from which the Rayleigh wave phase speed is obtained in the conventional SASW method:

$$c(\omega) \equiv \frac{\omega}{k} = \frac{\omega \Delta x}{\gamma}, \quad (5)$$

Δx being the spacing between the receivers. We are interested in the scattering coefficient β and its dependence on scattering geometry, frequency and the properties of the target. In particular, we want to determine whether or not it provides a unique "signature" of the target in the same sense that the depolarization function provides a unique signature in the case of electromagnetic induction.

Characteristically, ordnance items have a relatively simple shape: slender and axisymmetric on the scales of interest here. Coupled with the fact that we are in the scattering regime where k^{-1} is likely to be comparable to the size of the target, this suggests that UXO should have fairly simple characteristic scattering functions. The basic questions are (1) whether they are sufficiently different from the scattering functions of most clutter items to be useful for discrimination and (2) whether they can be adequately estimated from data collected in the field.

The scattering coefficient can be determined from phase shifts measured by the SASW technique. Rearranging equation (4) and using equation (5), we have

$$\mathrm{Re}\{\beta \exp[ik(x_1 + x_2 + 2x_T)]\} = \frac{\sin(\gamma_0 - \gamma)}{2\sin(\gamma)}, \quad (6)$$

where γ_0 is the phase shift that would be observed if there were no obstacle. It is determined by the dispersion relation:

$$\gamma_0 = \frac{\omega \Delta x}{c}, \quad (7)$$

and depends on the mechanical properties of the soil. The factor $\exp(i2kx_T)$ accounts for the phase shift that accrues as the wave travels from the far receiver to the target and back, while the factor $\exp[ik(x_1 + x_2)]$ simply establishes a phase reference at the sensor.

The scattering function includes the dependence on frequency and scattering geometry: β as a function of frequency (ω), the target depth (z) and orientation (θ, ϕ), and the sensor-target separation (r). Taking data from different angles (i.e., with the SASW device pointing towards the suspected target from different directions) samples the azimuth (ϕ) dependence. The frequency variation also samples elevation (θ) and depth (z) in some fashion. The question is whether or not, with an ω–θ sweep, enough of the parameter space ends up being sampled to support discrimination.

A simple numerical simulation for a homogeneous medium with an obstacle serves to demonstrate the basic principles. The basic arrangement is illustrated in figure 2. The simulation assumes that only surface waves of a constant velocity are present and that the amplitude of the reflected wave is given by a

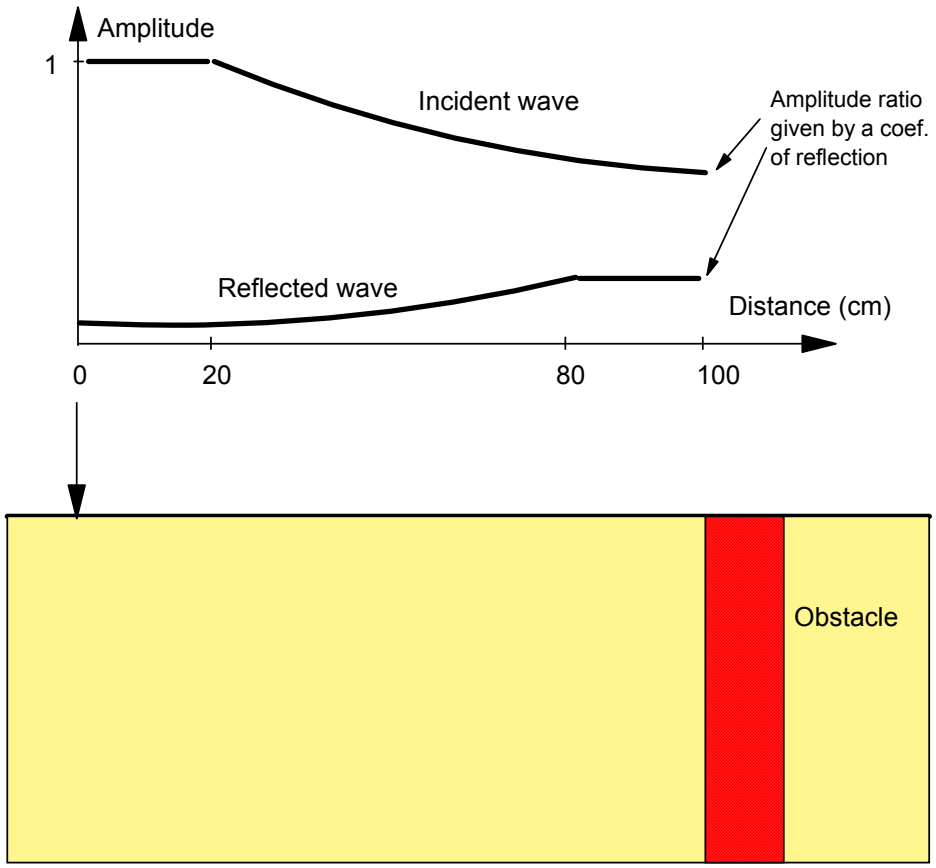

Figure 2. Schematic of numerical simulation model with obstacle at x = 100 cm. The amplitude of the reflected wave is determined by a reflection coefficient and attenuation follows a square root rule.

coefficient of reflection. Also, it is assumed that attenuation of the wave is based on a square root rule. The velocity of the medium was assumed to be 100 m/s. The phase velocity is calculated from the phase of the complex displacement curve using equation (5). Figure 3 shows the real part (in phase with the source) of the displacement as a function of x for reflection coefficients of 0.1, 0.2 and 0.3. The reflected waves do not have a very pronounced effect on the amplitude of the displacements at these levels. The effect is strongest nearest the obstacle, and is actually a reduction in the amplitude that increases as the reflection coefficient increases. For the imaginary part (out of phase with the source) of the displacement, the effect is reversed. The amplitude is increased rather than reduced, but by about the same magnitude. At one wavelength from the obstacle, there is about a 20% effect on the amplitude for a reflection coefficient of 0.3.

The phase shift effect is quite dramatic. It is manifested in apparent phase velocity fluctuations that vary with frequency, receiver spacing, reflection coefficient and distance to the obstacle. Figure 4 shows a composite surface plot of phase velocity as a function of frequency (f) and distance to the obstacle (x_T). This is the standard display for the Surface Wave for Obstacle Detection (SWOD) method, and shows the characteristic pattern of phase velocity fluctuations that indicates the presence of a buried object [3]. In this particular example, the reflection coefficient is 0.3 and the receiver spacing is 5 cm. There are very large (>50%) fluctuations in the apparent phase velocity as the obstacle is approached. The fluctuations are periodic in f and x_T, and are organized in a hyperbolic pattern: extrema and zero levels occur along lines with $x_T f$ = constant. This periodicity and characteristic pattern is due to the term

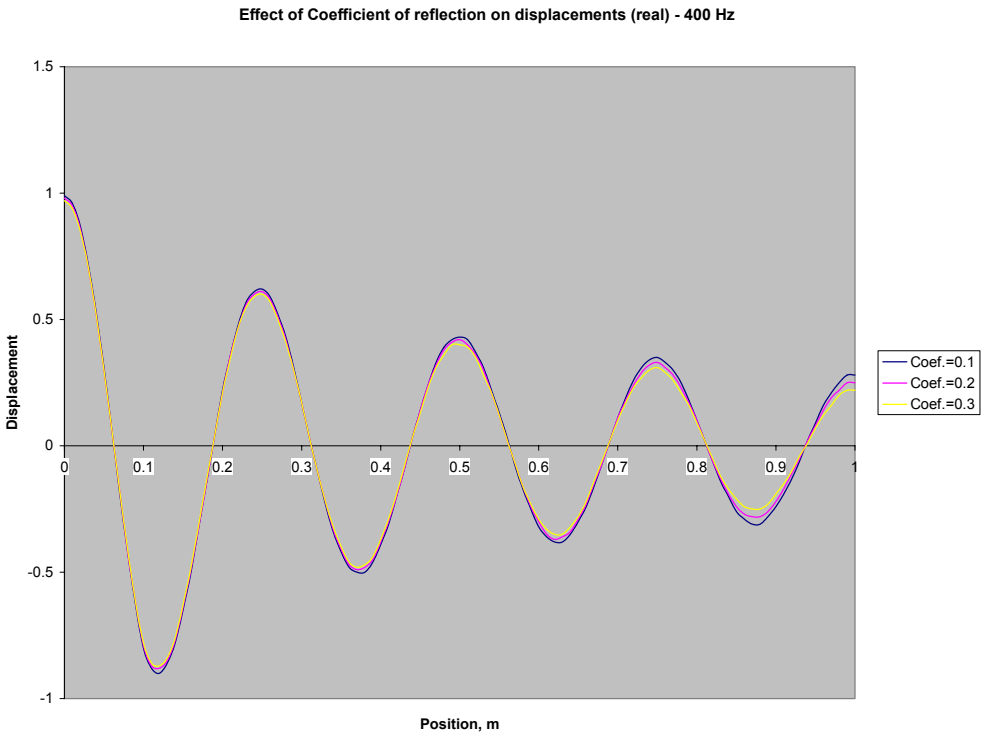

Figure 3. Real part (in phase with the source) of the displacement field as a function of position for reflection coefficients of 0.1, 0.2 and 0.3

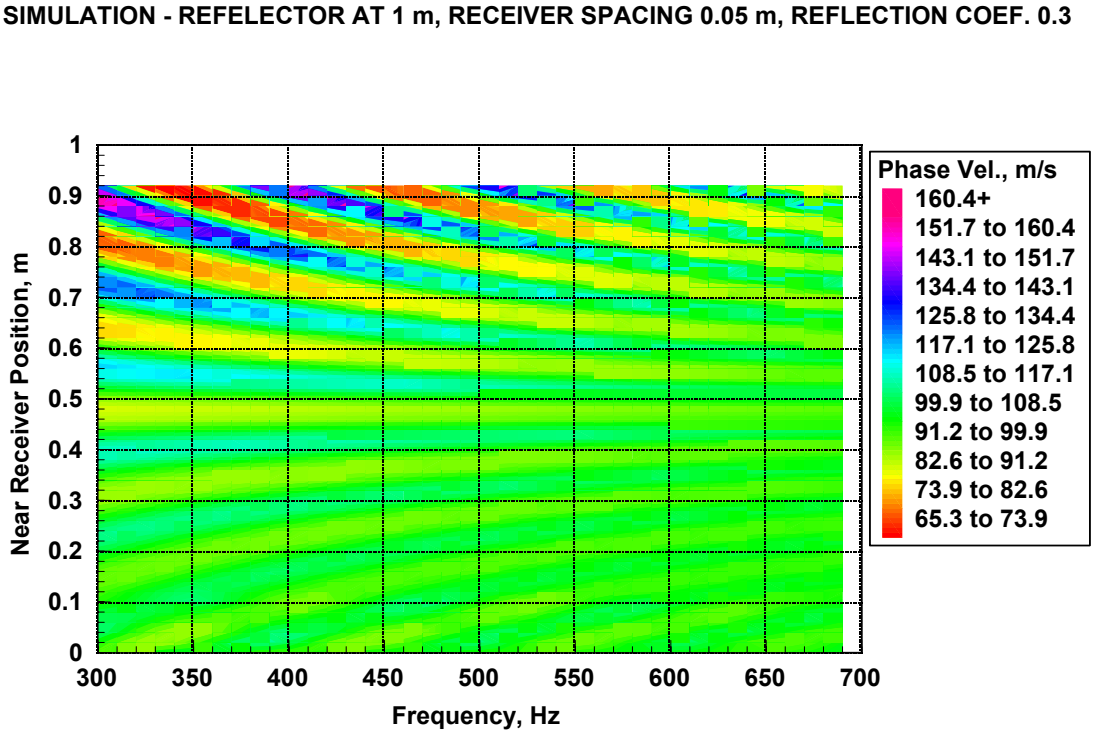

Figure 4. Dependence of the phase velocity fluctuations on frequency and distance to the obstacle.

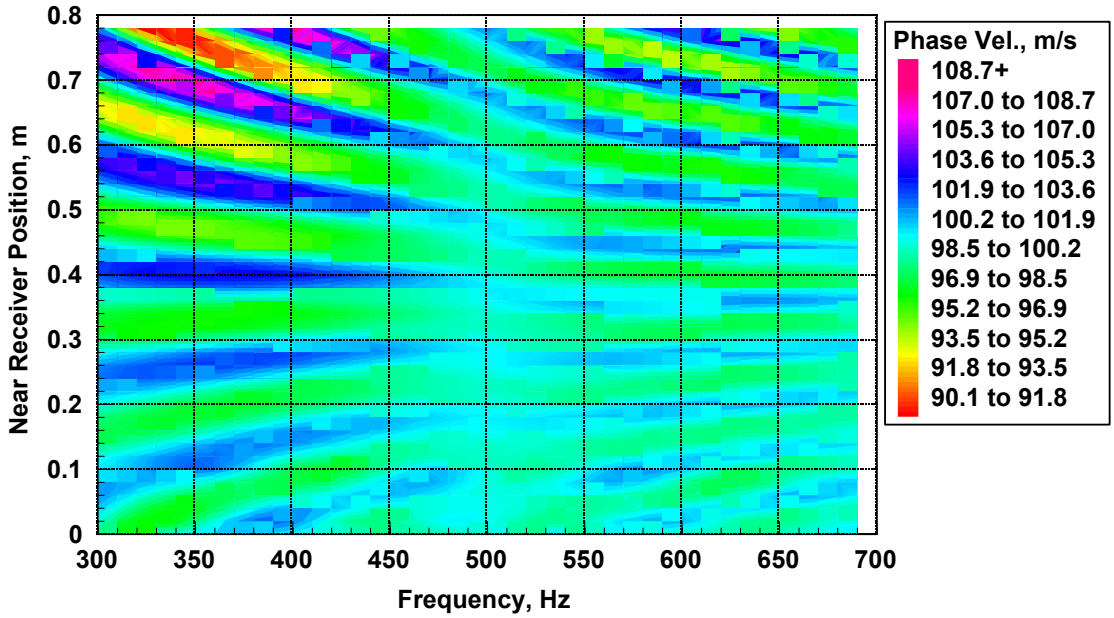

Figure 5. Same as figure 4, but with receiver spacing of 20 cm.

$$\exp[ik(x_1 + x_2 + 2x_T)] = \exp[i(2\pi f / c)(x_1 + x_2 + 2x_T)] \qquad (8)$$

in equation (4).

The pattern of fluctuations is a simple consequence of the measurement geometry. The strength of the fluctuations depends on the scattering coefficient and the receiver spacing. In this simulation, the obstacle is a simple vertical barrier. In general, the scattering coefficient will vary with frequency and depend on the size and shape of the object, its depth, and the orientation of the line over the object along which data are collected. The receiver spacing affects the phase velocity fluctuations via the competing terms in the denominator of the expression in equation (4). Figure 5 shows that the phase velocity fluctuations decrease substantially when the receiver spacing is increased from 5 cm (figure 4) to 20 cm (figure 5). Note, however, that the pattern of the fluctuations remains the same. As a rule, it is desirable to keep the spacing to half of a wavelength or less in order to fully resolve the phase fluctuations associated with the interference between incident and scattered waves. This turned out to be a shortcoming of the fixed-frame PSSA, which has a non-adjustable receiver spacing of 20 cm.

4. Experimental Work

The experimental work encompassed data collection for four objects buried in a soil bin. The work was conducted in the soil bin of the Rutgers University (figure 6). The bin, 4.2 m in diameter and 1.8 m deep, is filled with fine to medium sand. Along all the walls and the bottom there is an absorbing sawdust layer of about 30 cm thickness. The testing was conducted using the Portable Seismic Soil Analyzer (PSSA) The PSSA, shown in figure 6, is built by Geomedia Research and Development. It is a portable device for seismic testing of soil type materials. The device consists of an anvil type hammer and two accelerometers. The accelerometers are pneumatically coupled to the ground. Two different models are shown in figure 7. The original model, shown on the left, consisted of the hammer and accelerometer cylinders embedded into a frame with adjustable/sliding accelerometer holders. While the ability to have adjustable source to near receiver distance and receiver spacing was part of the original plan, the data were contaminated by frame oscillations. The manufacturer provided an alternative frame that reduced vibrations, but at the same time eliminated the potential for scalability of spacing between the source and receivers. The new frame, shown on the right, had a fixed source to the near receiver distance of 15 cm and a receiver spacing of 20 cm. The PSSA is fully controlled by a computer. During a single test, six impacts are applied and the signals are digitally recorded. Each record consists of 2048 samples at 100 kHz.

Figure 6. Soil bin at Rutgers University.

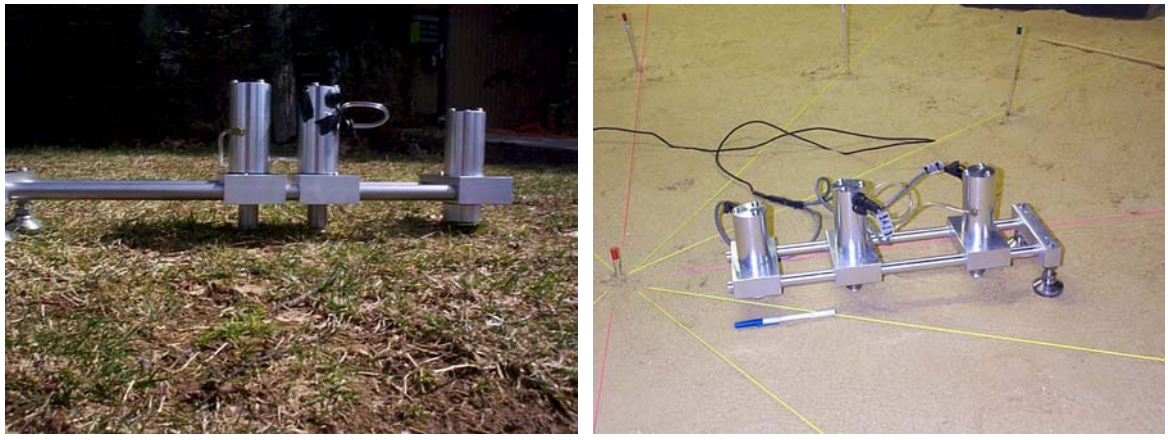

Figure 7. Portable Seismic Soil Analyzer. Adjustable frame model on left, fixed frame model on right.

Figure 8. Test objects. Clockwise from bottom: inert 105 mm projectile, ordnance fragment from the Badlands Bombing Range, and two pieces of clutter excavated at Fort A. P. Hill.

Four objects were chosen for testing. They are shown in figure 8. Object 1 is an inert 105mm projectile. Object 2 is a fragment of a larger ordnance item excavated at the Badlands Bombing range in Pine Ridge, South Dakota. Objects 3 and 4 are steel clutter items excavated from Firing Point 20 at Fort A. P. Hill in Virginia. These particular objects were chosen because in a previous study they were observed to have similar electromagnetic signatures. The test configuration is shown in figure 9. All the objects were placed with the top of the object 15 cm below the surface, and with the longitudinal axis in the direction of test line A. Bin testing was conducted along 6 test lines, A to F, in 30 degree increments. As it turned out, we were only able to collect useful data for objects 1, 2 and 3. During the course of the analysis we found that the frequency resolution (50 Hz) was really inadequate for our purposes, and attempted to collect the data for object 4 at a lower data rate. The data logging software did not work properly at the lower rate, and we ended up losing most of this data.

Testing along each test line was conducted using 10 cm increments. The starting point, position 0 cm, was a point where the distance between the far receiver and the center of the object was 100 cm. The center of every object matched the center of the bin. Six records are taken for every test point, each of 2048 samples. The sampling rate of the system is 100 Ks/s, providing a frequency resolution of about 50 Hz and the maximum frequency of about 50 kHz. It was anticipated that the maximum frequency of interest would be around 3 kHz.

Our analysis concentrated on observation of effects of buried objects on the dispersion of surface waves. In the standard SWOD testing procedure, the location of the source is fixed, and a closely spaced receiver pair is moved away from the source along a straight line. As described above, a buried object or cavity causes fluctuations in the dispersion curve. The fluctuations are caused by reflections of both surface and body waves from the obstacle. The intensity of fluctuations increases as the receiver spacing decreases and as the receiver pair approaches the obstacle. The fluctuations vanish once the receiver pair is on the far side of the obstacle from the source. If the receiver pair is placed to straddle the buried object, there is

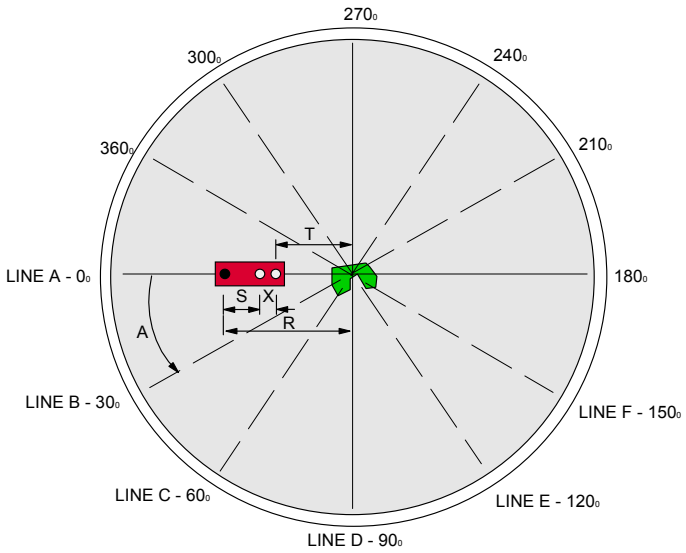

Figure 9. Test setup. Targets were buried with the top of the object 15 cm below the surface.

a general increase in the phase velocity of the dispersion curve for rigid obstacles, and a decrease for soft obstacles or cavities. With the PSSA, we have a fixed source/receiver configuration that is moved along a straight line collecting data. Here, once the device has completely passed over the object so that the source and receivers are all on the same side, we will see phase velocity fluctuations that die out with distance from the object in a pattern similar to the pattern in figures 4 and 5.

Figure 10 shows typical signals from the two receivers for six successive hammer strikes. The signals are quite repeatable. Near receiver time histories for Objects 1, 2 and 3 are compared to the time histories for the bin without buried objects in figure 11. The waveforms have been normalized at the peak, and the data are displayed as color maps. Time is along the horizontal axis, distance along the line over the target is along the vertical axis. Normalized amplitude is color-coded. Negative amplitudes are blue and violet, positive amplitudes are yellow and red. Note that, although the time resolution is 0.00001 sec, the spatial resolution is only 10 cm. The interpolated amplitude maps give the appearance of higher spatial

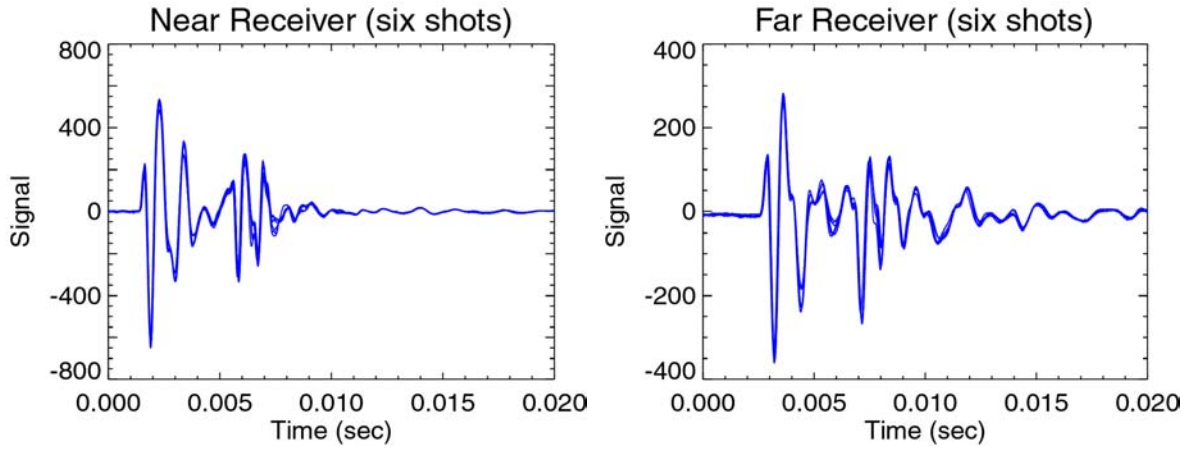

Figure 10. Sample signals from six successive hammer strikes measured by the two receivers

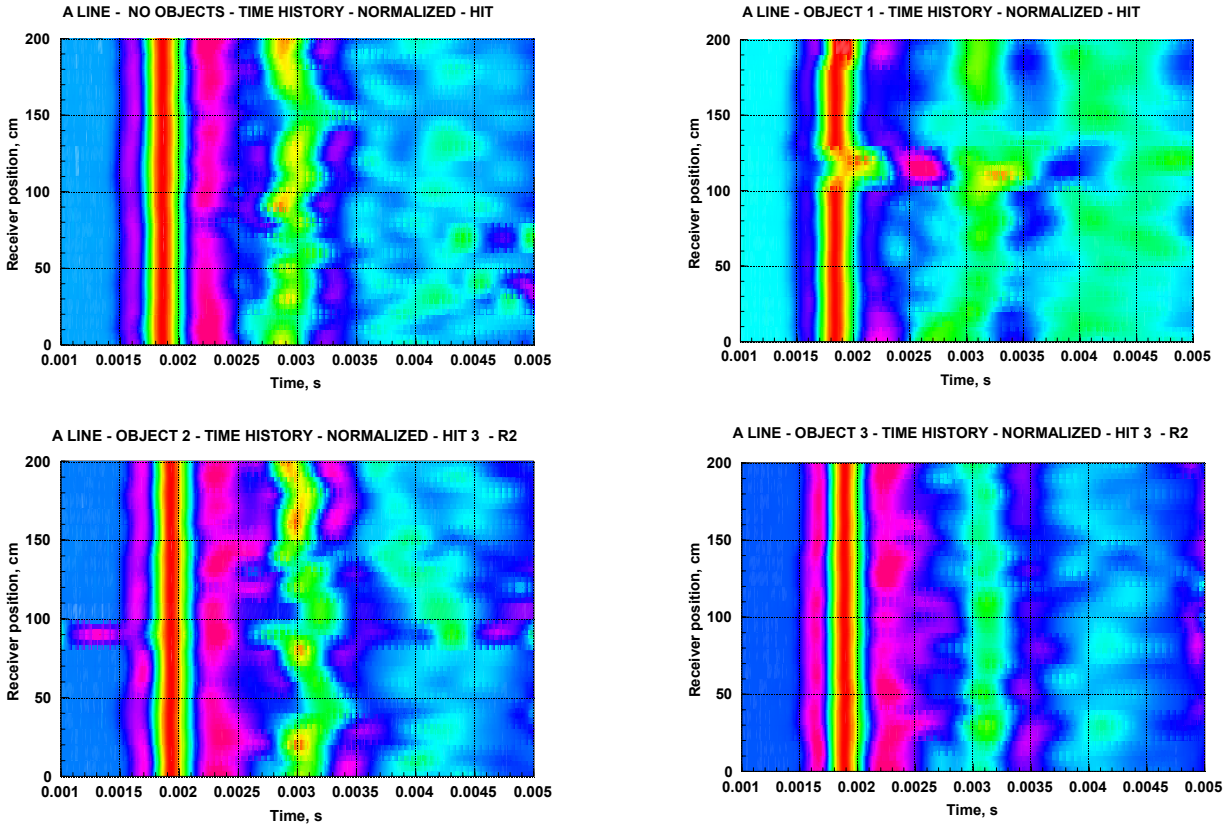

Figure 11. Time histories along lines over Objects 1, 2 and 3, and with no object in the bin.

resolution. Other than artifacts due to the occasional time glitch (e.g. the apparent offset of the peak for Object 1 at 120 cm) there is very little spatial structure in the data. In particular, there is no clearly identifiable effect of the object on the signal amplitude. This is confirmed with plots of frequency spectra along lines over the targets.

Dispersion curves were generated from the phase of the cross power spectra of the PSSA data. The process is illustrated figures 12 and 13. These are screen shots of the program developed at Rutgers for use with the PSSA. In the first part of the dispersion curve development, the average cross power spectrum and coherence are calculated from records for six hammer hits. Typical auto power spectra, cross power spectrum magnitude and phase and coherence are shown in figure 12. The frequency scale is from 0 to 3 kHz with major divisions every 500 Hz. The auto spectra for the two receivers are shown in the upper left as functions of frequency to 3 kHz. The cross spectrum magnitude is shown in the lower left panel. The coherence is in the upper right, and the phase is in the lower right panel. Note that at the frequency resolution of 50 Hz, the phase is ambiguous below a few hundred Hz, i.e., it is not possible to separate phase fluctuations from wrapping around 360 degrees in this at these frequencies. The cross power spectrum is transformed from the "wrapped" into a continuous format, as shown in figure 13. Note that only frequencies of 400 Hz and higher are displayed because of the resolution problem noted above. The wrapped (mod 360 degrees) phase is shown in the upper left. The coherence is in the lower left. Unwrapped phase (also flipped in sign) is shown in the upper right panel. From the "unwrapped" phase the phase velocity is calculated from the known receiver spacing and frequency using equation (5). It is shown in the lower right panel. In standard SASW testing, only portions of the dispersion curve where

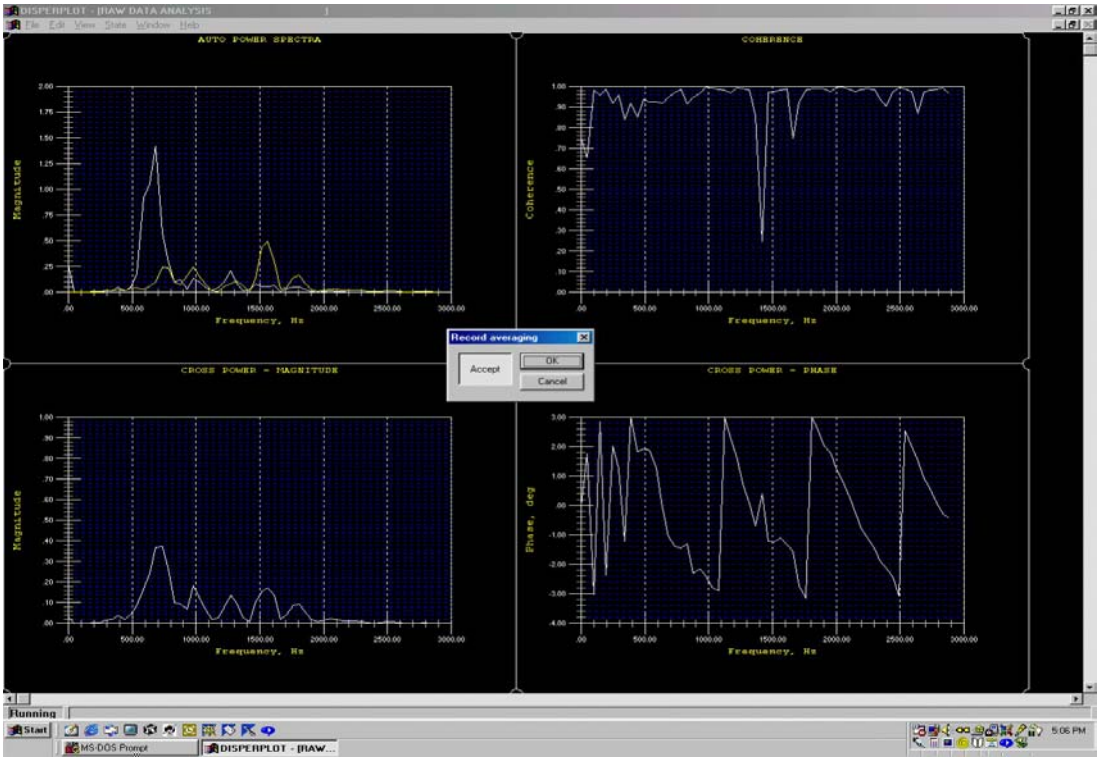

Figure 12. Cross power spectrum and coherence template.

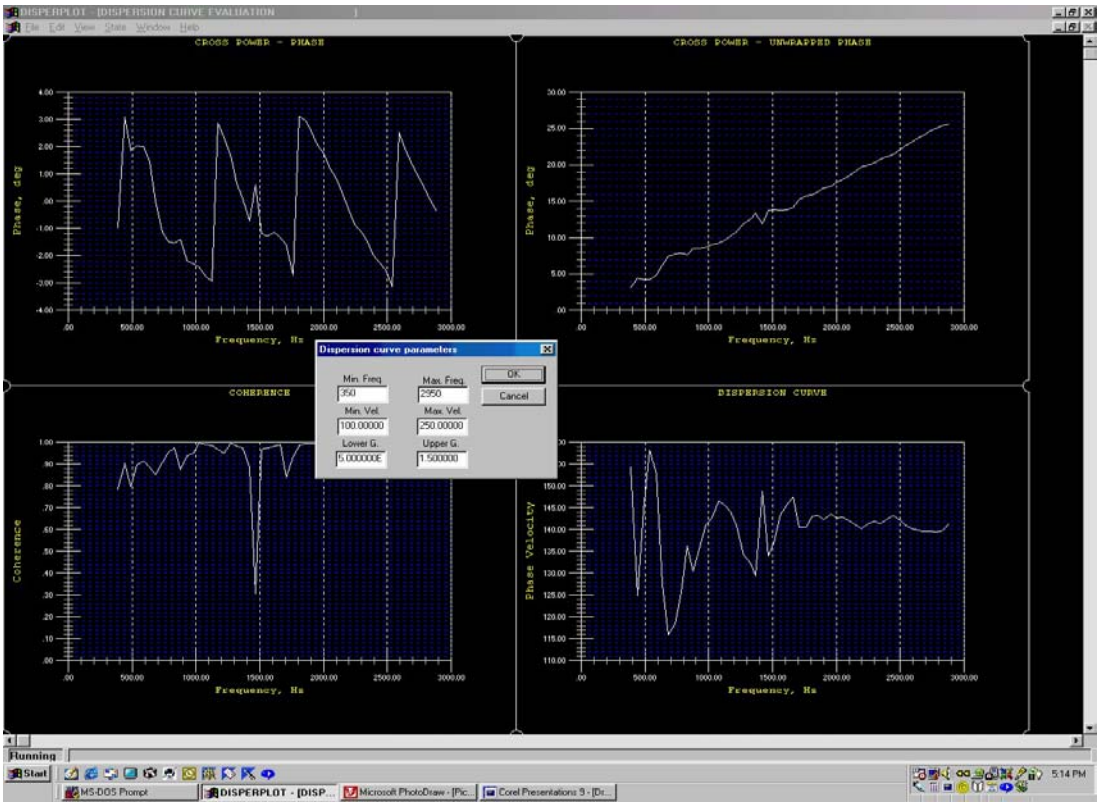

Figure 13. Dispersion curve template.

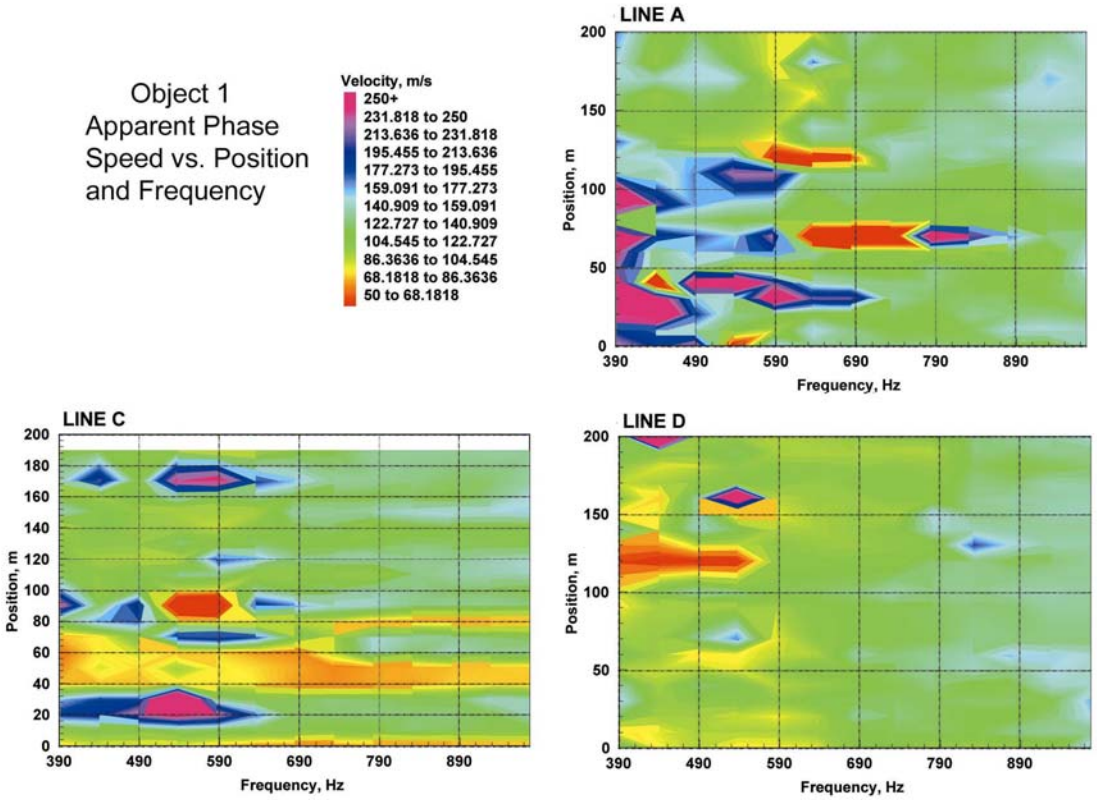

Figure 14. Dispersion surfaces (apparent phase speed as a function of position and frequency) along various lines over object 1.

coherence exceeds a certain threshold are considered. Since it is not clear at this stage how buried objects are affecting the coherence, the coherence was ignored in the development of dispersion curves.

Dispersion surfaces for Object 1 (105 mm projectile) are shown in figure 14. The dispersion surface is a map of the apparent phase velocity as a function of frequency and far receiver position along a line over the object, which is located at 1.0 m. Line A is parallel to the long axis of the projectile, line D is perpendicular to the long axis, and line C is 30 degrees off perpendicular. Along line A there are strong velocity variations in front of and above the object at frequencies less than 700 or 800 Hz, corresponding to wavelengths greater than about 20 cm at the nominal phase velocity of 150 m/sec. Recall that the depth to the top of the object is 15 cm. The velocity fluctuations are quite strong, >65%. The spatial (10 cm) and frequency (50 Hz) resolution is not good enough to unambiguously relate the pattern of the velocity fluctuations to surface wave scattering. Along line C there are similar velocity fluctuations in front of the object, but also some structure behind it. The velocity fluctuations are much weaker along line D. The results are clearly ambiguous. Some of the anomalous velocity fluctuations can be correlated with low coherence between the signals at the two receivers, but the causes of such low coherence have not been identified. Results for the other objects are similarly ambiguous.

Field testing was conducted to evaluate effects of soil heterogeneity on the surface wave dispersion, as evaluated by the PSSA. The testing was conducted on grassy areas in front of the Civil Engineering Department building (figure 15). A comparison of the field and bin dispersion curves is shown in figure 16. The plots each show apparent phase speed as a function of frequency at five locations. Bin results for line A over object 1 are shown on the left. The individual curves are for data collected with the far

receiver at locations of 40, 50, 60, 70, and 80 cm. Recall that the object is centered at the 0 cm location. Five traces at different locations in the field (with no object present) are shown in the plot on the right. The frequency scales run from 350 Hz to 1500 Hz, with major increments on the plots at 200 Hz intervals. The phase velocity scale for the bin data is 0 to 300 m/sec, and is 0 th 150 m/sec for the field data. Two important differences can be observed. Dispersion curves for bin testing with an obstacle have significant fluctuations in the frequency range previously identified as the range of anticipated disturbances, 350-700 Hz. The strength of the fluctuations increases as the object is approached. The phase velocity fluctuations in the field are not nearly as pronounced, and appear typical of what is usually obtained from SASW soil testing.

Figure 15. Field testing with the PSSA outside the Civil Engineering building at Rutgers.

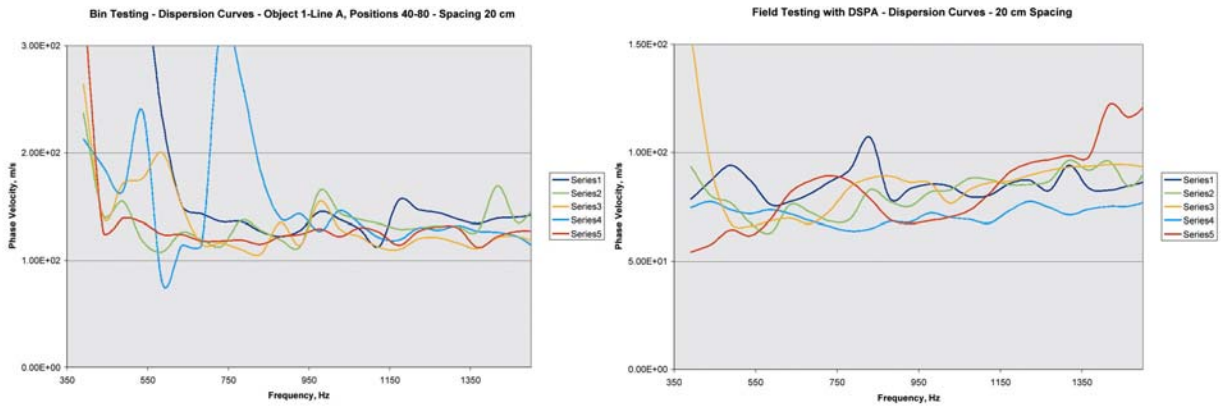

Figure 16. Dispersion curves from soil bin testing with an object present (left plot) and from open ground outside the Civil Engineering building at Rutgers (right plot).

5. Conculsions

The Spectral Analysis of Surface Waves (SASW) seismic test is routinely used to determine mechanical properties of soil and pavement structures. The test instrumentation consists of an impact source and a pair of seismic receivers. In the standard test, soil mechanical properties are estimated from the phase velocity dispersion relation that is calculated from the frequency-dependent phase shift between the signals measured at the two receivers. When there is a buried object close by, interference between the primary and backscattered waves results in fluctuations of the apparent phase speed as a function of frequency and location of the sensors relative to the object. The objective of this project was to demonstrate that SASW technology can be used to discriminate between buried UXO and clutter. Our approach involved measurements on UXO and clutter items in the Rutgers University soil bin using a commercial soil testing unit. We collected data using the Portable Seismic Soil Analyzer (PSSA), which consists of an anvil hammer and two accelerometers pneumatically coupled to the ground. We were able to measure phase velocity fluctuations at low frequencies in front of UXO and clutter targets. Unfortunately, the frequency and space resolution of the measurements (50 Hz and 10 cm, respectively) were not good enough to adequately resolve the pattern or obtain quantitative estimates of reflection coefficients. Consequently, the results are inconclusive. Although there is qualitative evidence of an exploitable phenomenon, we were not able to quantitatively evaluate the potential for UXO/clutter discrimination.

6. References

[1] Nelson, H. and J. McDonald, “Multisensor Towed Array Detection System for UXO Detection,” *IEEE Trans. Geoscience and Remote Sensing, 39*(6), June 2001, 1139-1145. Carin, L., et al, “On the Wideband EMI Response of a Rotationally Symmetric Permeable and Conducting Target,” *IEEE Trans. Geoscience and Remote Sensing, 39*(6), June 2001, 1206-1213. Bell, T., et al, “Subsurface Discrimination Using Electromagnetic Induction Sensors,” *IEEE Trans. Geoscience and Remote Sensing, 39*(6), June 2001, 1286-1293. Tantum, S. L. and L. M. Collins, “A Comparison of Algorithms for Subsurface Target Detection and Identification Using Time-Domain Electromagnetic Induction Data,” *IEEE Trans. Geoscience and Remote Sensing, 39*(6), June 2001, 1299-1306.

[2] Krumhansl, P., et al, "Innovative seismic system for buried UXO detection and classification," Partners in Environmental Technology, Technical Symposium and Workshop, Arlington, Virginia, December 1998 & November 1999. Krumhansl, P., et al, “Development and Controlled Testing of a Seismic System for UXO Classification,” UXO/Countermine Forum, New Orleans, Louisiana, April 2001.

[3] Gucunski, N., V. Krstic and A. Maher, “Field Implementation of the Surface Waves for Obstacle Detection (SWOD) Method,” 15th World Conference on Non-Destructive Testing, Rome, October 2000.

[4] Ganji, V., N. Gucunski and A. Maher, "Detection of underground obstacles by SASW method – Numerical aspects," *J. Geotechnical and Geoenvironmental Engin. 123*(3), 212-219, 1997.